Iranian Journal of Materials Forming 12 (2) (2025) 42-57

Online ISSN: 2383-0042

IJMF

Iranian Journal of Materials Forming

Journal Homepage: http://ijmf.shirazu.ac.ir

Research Article

Residual Stress Analysis in Milled DIN 1.2344 Die Casting Mold: A Fusion of Numerical Simulation and XRD Experimental Validation

R.A. Mahdavinejad* and S.M. Sedehi

School of Mechanical Engineering, College of Engineering, University of Tehran, Tehran, Iran

ARTICLE INFO

Article history:

Received 29 January 2025
Reviewed 4 March 2025
Revised 3 April 2025
Accepted 5 April 2025

Keywords:

Residual stress
Milling
DIN 1.2344 steel
Die-casting mold

Please cite this article as:

Mahdavinejad, R. A., & Sedehi, S. M. (2025). Residual stress analysis in milled DIN 1.2344 die casting mold: A fusion of numerical simulation and XRD experimental validation. *Iranian Journal of Materials Forming*, *12*(2), 42-57. https://doi.org/10.22099/IJMF.2025.52296.1322

ABSTRACT

Milling is one of the most widely used processes in the manufacturing of die-casting molds and other industrial molds. A major challenge in this process is the generation of residual stresses on the workpiece surface, which can lead to distortions and compromise the precision and performance of the mold. This study investigates the residual stresses induced by milling DIN 1.2344 steel, utilizing the Taguchi design of experiments (L9 array) and validating the results experimentally through X-ray diffraction (XRD) tests. The study examines the effects of three primary milling parameters, cutting speed, feed rate, and depth of cut, on residual stresses and identifies the optimal conditions for minimizing these stresses. The results indicate that increasing the cutting speed from 50 to 112.5 m/min reduces tensile residual stresses by 22%. Additionally, increasing the feed rate from 10 to 20 mm/s leads to an 18% reduction in residual stresses; however, further increases beyond this threshold lead to stress amplification. Regarding the depth of cut, increasing it from 0.2 to 0.4 mm causes a 15% rise in residual stresses, while a depth of 0.6 mm results in a 10% reduction. Furthermore, the cutting forces F_x and F_z initially increase moderately with cutting speed but decrease at 112.5 m/min, attributed to thermal softening effects. These findings offer valuable insights for optimizing the milling process and improving the quality of machined components in the mold-making industry.

1. Introduction

Die-casting is a highly efficient and widely adopted method for mass-producing industrial components. Its popularity stems from several advantages, including the ability to create complex shapes with high accuracy in a short time frame. The high production speed of die-casting leads to significantly lower manufacturing costs. Furthermore, components formed using this process often display enhanced mechanical properties compared to those made with other casting techniques, primarily due to the high hydrostatic pressure exerted during production. This pressure-based technique enables the fabrication of thin-walled, sharp-edged, and smooth-surfaced parts under controlled conditions [1]. The longevity of a die-casting mold is largely influenced by the material selection, including its chemical

* Corresponding author
E-mail address: mahdavin@ut.ac.ir (R.A. Mahdavinejad)
https://doi.org/10.22099/IJMF.2025.52296.1322

composition, manufacturing process, and heat treatment. Repeated exposure to fluctuating temperatures induces thermal stress, which gradually deteriorates the mold's structural integrity [2]. This degradation typically begins as fine cracks caused by thermal cycling, which can evolve into more significant fractures over time. Such crack-related failures are a critical factor in determining the service life of a die-casting mold. Consequently, mold material must possess high thermal resistance and be able to withstand operational demands without sudden breakdowns [3]. Despite technological advancements, conventional machining techniques—such as turning, milling, and drilling—remain vital in shaping steel components. This ongoing reliance has prompted extensive theoretical and experimental studies in steel machining. Efforts to minimize machining costs, enhance tool durability, and improve surface finish underscore the necessity for continued research in this domain [4]. Among the various machining processes involved in die-casting mold fabrication, milling holds particular significance. In recent years, advancements in numerical control systems and cutting tool technologies have enhanced milling's capabilities, enabling it to effectively address the challenges inherent in mold production. Owing to its high versatility, milling is especially suited for shaping complex geometries, making it a favored method in industrial mold manufacturing. Despite its advantages, milling introduces residual stresses into the mold structure, which can significantly impact both dimensional and geometric accuracy, as well as the mold's service life. Precision in mold manufacturing is essential to ensure that the dimensions tolerances of die-cast components remain within specified limits. Moreover, the machining of critical mold features such as parting lines and sliding elements requires exceptional accuracy to ensure smooth operation and effective sealing between components. Residual stresses generated during milling can result in dimensional and geometric deviations. Over time, the gradual release or redistribution of these residual stresses may cause distortion or warping in the mold. In addition to dimensional stability, such stresses can negatively affect properties like fatigue life and corrosion resistance. The development of residual stresses is influenced by a wide range of factors, many of which are difficult to monitor or regulate precisely. However, key machining parameters namely cutting speed, feed rate, and depth of cut are relatively easy to adjust. Determining the optimal combination of these variables is essential for minimizing residual stress and achieving stable, high-precision machining results. A review of current literature reveals that the optimal cutting speed, feed rate, and depth of cut for minimizing residual stress are highly dependent on the material being machined. For each material, specific values for these parameters can be identified to achieve minimal residual stress during milling operations. In a 1995 study, Fuh et al. [5] experimentally investigated residual stresses generated in the milling of Al2014-T6 alloy. They employed response surface methodology and Taguchi methods for experimental design, comparing the outcomes from both approaches. To isolate the effects of quantitative variables, qualitative factors—such as lubrication and inherent material properties—were kept constant, while variables such as tool geometry, cutting conditions, and material hardness were systematically varied. The study found that tensile residual stresses were present in the outermost layer of the machined surface, increasing rapidly with depth before transitioning to compressive stresses at greater depths. Notably, residual stress levels initially decreased with rising cutting speed, began to increase again beyond a certain threshold. Demirpolat et al. [6] emphasized the industrial significance of wrought aluminum alloys, citing their low density, high strength, corrosion resistance, machinability, and recyclability. Their comprehensive study focused on optimizing machining parameters—such as tool wear, surface finish, and process stability with the aim of enhancing performance and reducing production costs. Similarly, Liang et al. [7] conducted simulations to analyze residual stresses during the machining of AISI 316L and AISI 4340 steels. Their work considered the influence of material properties, initial temperature of the workpiece, and cutting forces on residual stress development. Research findings indicate that increasing the feed rate results in a larger cutting zone during milling. One of the

significant parameters explored in this context is the tool's cutting-edge radius. As the cutting-edge radius increases, the region under compressive residual stress expands, pushing the compressive stress zone deeper beneath the machined surface. Honarpisheh and Mansouri [8] experimentally investigated the residual stress distribution in TIG-welded CK45 steel sheets using the contour method, emphasizing the thermal effects of welding at 600 °C for 10 hours. Mohammadpour et al. [9] investigated how machining parameters affect residual stress during the turning of AISI 1045 steel. Their findings showed that both cutting speed and feed rate initially caused an increase in maximum residual stresses. However, this trend reversed beyond a certain speed, where tensile residual stresses began to dominate. Similarly, Stenberg et al. [10] performed numerical simulations to analyze patterns during the turning of 20NiCrMo5 steel. They observed that residual stress distribution along the direction perpendicular to the machined surface exhibited a transition from tensile to compressive stress, which then remained stable. Interestingly, at high feed rates, residual stresses became relatively unaffected by further changes in feed rate. Their study also indicated that elevated cutting speeds resulted in reduced surface residual stresses and a more uniform compressive stress profile through the workpiece depth. Another notable finding was that zero or negative rake angles promoted tensile residual stress formation on the machined surface. Kara et al. [11] explored the interplay between residual stresses, machining parameters, and performance during the milling of compacted graphite iron (CGI). Using X-ray diffraction (XRD) to measure stress on both cast and machined surfaces, and employing cutting force modeling to assess tangential force, power, and work done, they concluded that machined surfaces predominantly exhibited tensile residual stresses. These were attributed to the mechanical and thermal loading conditions inherent to the milling process. Their study also highlighted that reducing feed rate effectively minimized plastic deformation, thereby lowering residual stress levels. An increase in cutting speed generally leads to elevated temperatures during machining. However, the reduced contact time between the tool and the workpiece limits excessive heat accumulation. At lower feed rates, residual stresses tend to increase, whereas at higher feed rates, increasing cutting speed results in a reduction of residual stresses. This interplay between cutting parameters and residual stress underscores the critical importance of optimizing machining conditions to enhance the fatigue strength of compacted graphite iron CGI components. These insights contribute significantly to process optimization and quality control in CGI milling applications.

Zhou et al. [12] recognized the necessity for comprehensive residual stress data to optimize the machining of thin-walled components. To address this, they developed a reverse analysis method for determining residual stress profiles during the milling of Ti-6Al-4V alloy, based on the deformation observed in thin sheets. Their approach utilized a hyperbolic tangent function to represent the stress profile and established a correlation between this profile and the degree of sheet bending. An algorithm was then introduced to calculate the stress profile parameters from measured deformation. The method was validated through six test groups, achieving a prediction accuracy exceeding 90.19%. This reverse modeling technique allows for rapid estimation of residual stress profiles by measuring deformation in thin, machined components. Fergani et al. [13] explored how milling-induced residual stresses influence distortion in Al7075 components. They employed X-ray diffraction for stress measurements and validated their findings against simulation results. The study revealed that the highest tensile residual stresses were located near the surface, gradually diminishing with depth and transitioning into compressive stresses in the subsurface layers. Several other studies have employed the Taguchi method for statistical analysis of machining parameters, focusing on their impact on cutting forces, surface roughness, tool wear, and tool life [14, 15]. Pınar et al. [16] employed the Taguchi method to compare different cooling techniques in the pocket milling of AA5083-H36 aluminum alloy. By analyzing the effects of machining parameters on surface

roughness, they demonstrated that cooling method selection significantly influences the final surface quality. Zahoor et al. [17] investigated the impact of forced spindle vibrations on surface roughness, dimensional accuracy, and tool wear during the vertical milling of AISI P20 steel. Their results revealed that increased vibration amplitude leads to significant deterioration in surface finish and dimensional precision, highlighting the importance of dynamic stability in high-precision machining. The novelty of the present research lies in its integration of numerical simulation with experimental analysis to investigate the effects of the milling process on residual stress distribution and machining forces in die-casting molds. Unlike earlier studies that primarily addressed residual stresses in a general context, this work systematically examines how these stresses vary with different machining parameters, presenting an accurate model to identifying parameter ranges. Additionally, this study is the first to analyze how chip formation mechanisms and thermomechanical effects influence machining forces and, subsequently, residual stress development. By deepening the understanding of stress-inducing phenomena in the milling of die-casting molds, this research offers actionable insights for optimizing milling conditions, ultimately aiming to improve dimensional accuracy, minimize distortion, and extend mold lifespan.

2. Materials and Methods

This study focuses on the DIN 1.2344 alloy, commonly referred to as H13 in American standards, a hot-work tool steel for its balanced combination of hardness, toughness, and resistance to thermal shock. The alloy's composition includes substantial amounts of chromium, molybdenum, and vanadium, which contribute to its high wear resistance and thermal stability. These properties make it particularly suitable for industrial applications involving elevated temperatures and intense mechanical loads, such as pressure die-casting molds, extrusion dies, and hot forging tools. Its excellent hardenability and strong resistance to thermal cracking also make it a preferred material in the automotive, aerospace, and precision metal component industries.

This research employs both experimental and numerical simulation methods to assess the alloy's behavior under various milling conditions. In the experimental phase, DIN 1.2344 specimens were subjected to milling using different cutting parameters. For the simulation phase, numerical models were developed to analyze stress distribution, material deformation, and the influence of cutting conditions on overall machining performance. The combined findings from both approaches provide valuable insights into optimizing the milling process for this alloy, with the potential to significantly extend tool life and improve process efficiency.

2.1. Experimental procedure (machining and XRD)

The milling experiments on DIN 1.2344 alloy were conducted using five distinct parameter sets to evaluate the influence of key machining variables on various performance metrics. Specifically, the effects of cutting speed, feed rate, and depth of cut were examined, as summarized in Table 1. Cutting speed ranged from 62.5 to 125 m/min, with corresponding feed rates increasing from 6.66 mm/s at the lowest speed to 33.33 mm/s at the highest. The depth of cut was varied across five levels, from 0.05 to 0.5 mm. These parameters selected for their combined impact on machining forces, tool wear, and surface finish. All experiments were performed on a CNC milling machine, with real-time measurements of cutting and feed forces. Surface roughness was also assessed under each parameter set to determine how the combined conditions influenced the final surface quality

Table 1. Design of experiment (DOE) parameters used in milling of DIN 1.2344 alloy

Experiment No.	Cutting speed (m/min)	Feed rate (mm/s)	Cut depth (mm)	Level 1	Level 2	Level 3
1	62.5	6.66	0.05	1	1	1
2	87.5	13.33	0.10	1	2	1
3	100	20	0.30	2	1	1
4	112.5	26.66	0.40	2	2	2
5	125	33.33	0.50	3	3	2

of the machined workpieces. The experimental findings provide a foundation for optimizing milling parameters to improve both process efficiency and surface integrity during the machining of DIN 1.2344 alloy under different operating conditions.

2.2. Residual stress measurement using XRD

Residual stress measurements in this study were performed using the X-ray diffraction method. Due to the dimensional limitations of available XRD equipment—specifically, a maximum sample length and width of 18 mm and a thickness not exceeding 3 mm—machining workpieces to meet these constraints posed significant challenges. Milling thin parts presents particular difficulty, especially with secure clamping during the machining process.

To address this, DIN 1.2344 alloy blocks measuring of 20 × 25 × 32 mm were initially prepared. These dimensions were chosen to match the clamping fixture jaws, ensuring stability during milling with minimal vibration and optimal surface quality. Prior to machining, the samples underwent a stress-relief annealing process, a common thermal treatment used to eliminate internal stresses and improve material stability and mechanical properties. This process is commonly applied to metals and other solid materials to eliminate internal stresses and structural changes, thereby transforming the material into a more stable form with enhanced mechanical properties. In the next step, the workpieces were clamped from the side with the lowest thickness and subjected to step milling operations to achieve final dimensions of 18 mm in length and width, and 2.3 mm in height. In the XRD test, measurement accuracy was evaluated through repeated trials. The average standard deviation in the measurement of crystallographic parameters was less than 2%, indicating high precision. Additionally, comparison of the XRD results with reference values from ASTM standards, which provide practical guidelines for calculating residual stress based on peak displacement in diffraction patterns, showed that the discrepancy in residual stress calculations was less than 3%. These results demonstrate that both the numerical and experimental methods employed in this study are highly accurate and reliable. The final part obtained through this process is shown in Fig. 1.

The machining scenario is as follows: in the final milling stage, residual stress measurements are performed. The upper step surface is milled using specific cutting speed, feed rate, and cutting depth parameters to analyze the residual stress on that surface. The height of the upper step on the workpiece corresponds to the cutting depth for each sample. For every case, this height is adjusted so that, after the final milling operation, the remaining thickness of the sample is 3 mm. Since the fourth stage represents the main phase of the milling process and residual stress measurements are conducted on the surface produced in this step, it is essential to carry out the milling with maximum precision and under near-ideal conditions.

Key factors in achieving this include precise control of machine and tool vibrations, maintaining the optimal condition of the tool's cutting edges, and ensuring accurate alignment of the workpiece within the fixture. Fig. 2 illustrates the milling operation conducted on the workpiece.

To ensure uniform cutting depth across the entire height of the step and to improve the accuracy of the alignment process, an indicator gauge was used to align the workpiece along both the Z and Y axes. The separation of the sample for residual stress measurement via XRD was performed using wire-cutting. It is important to note that the wire-cutting operation was carried out on the side opposite to the milled surface, ensuring it was sufficiently distant from the area where residual stress measurements were to be taken.

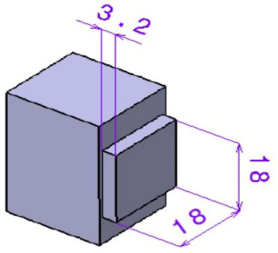

Fig. 1. Step created on the block through milling to obtain final sample dimensions for XRD measurement.

Fig. 2. Milling procedure for preparing the upper step surface of the workpiece.

This precaution ensures that the opposite step surface does not influence the residual stress readings. The residual stresses induced by the wire-cutting process are superficial and do not extend deeper than 3 mm, thus having no effect on the measurement area. The size of the final piece was determined based on the size limitations of the XRD machine. The piece has two key surfaces: the upper face, created by milling, where residual stress measurement is performed, and the lower face, created by the wire-cutting process. The rear surface, which is the one created by wire-cutting, is placed on the XRD machine stage, so it must meet appropriate smoothness standards. Although wire-cutting generally produces adequately smooth surface, surface quality can influence measurement accuracy and should be carefully considered. For this experiment, all samples had sufficient smoothness and did not require any additional corrective procedures. Fig. 3 shows the final piece after being separated by wire-cutting.

2.3. Residual stress calculation via XRD testing

Residual stresses are internal stresses that remain in a material after the removal of external loads. These stresses significantly impact properties such as dimensional stability, corrosion resistance, and fatigue life. Present in nearly all manufacturing processes, they must be carefully controlled in critical components, as excessive or uneven residual stress can cause distortion, dimensional changes, or even failure. On the other hand, compressive residual stresses can be beneficial, as they help prevent crack propagation under cyclic loading. X-ray diffraction is a non-destructive technique used to measure surface residual stresses by analyzing changes in the spacing of crystalline planes (denoted as d). Under tensile stress, d increases, shifting diffraction peaks to lower angles, whereas under compressive stress, d decreases, shifting peaks to higher angles.

While XRD is applicable to a wide range of materials, including metals and composites, its measurement depth is limited to a few microns. Accurate XRD data analysis requires specialized software and an in-depth understanding of diffraction peak shifts. Because multiple factors can influence the measurements, XRD is often complemented by other methods—such as finite element modeling—for a more complete understanding of residual stress distributions. The principle behind XRD is the measurement of lattice spacing changes, which reflect internal stress. These changes alter the positions of diffraction peaks, allowing calculation of the magnitude and direction of residual stresses. To determine the correct orientation for strain measurements, the crystal coordinate system must be considered. Assuming that σ_3 and ε_3 are perpendicular to the sample surface and that $\sigma_3 = 0$ (even though ε_3 may not be zero), ε_3 can be derived from the 2θ position in the diffraction pattern using Bragg's law. The spacing value d_n is then calculated using established relations. Fig. 4 illustrates the crystal coordinate system used for strain measurements, showing the measurement direction the orientation of diffraction planes parallel to the surface, and the related strain formula (Eqs. (1) and (2)).

$$n\lambda = 2\acute{d}\ \sin\theta \tag{1}$$

$$\varepsilon_3 = \frac{d_n - d_0}{d_0} \tag{2}$$

The interplanar spacing can be measured at the tilt angle ψ by rotating the sample along the $d_{\varphi\psi}$ direction using the device's goniometer.

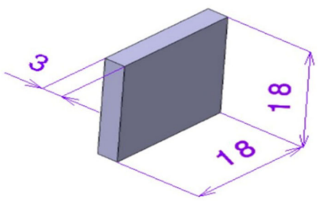

Fig. 3. The final part used in the XRD test.

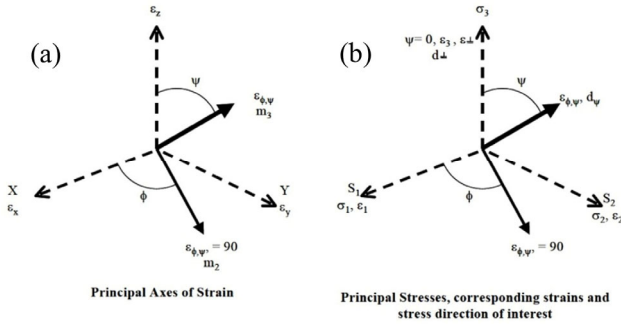

Fig. 4. (a) Crystallographic coordinate system in which strain is measured, (b) the direction for strain measurement and the planes parallel to it.

$$\varepsilon_\Psi = \frac{d_{\emptyset\Psi} - d_0}{d_0} \tag{3}$$

Given that the stress is stored elastically within the material, Hooke's law can be applied:

$$\sigma_y = E\varepsilon_y \tag{4}$$

Considering that the sample's surface is free, it is reasonable to assume that $\sigma_z = 0$. This implies a plane stress condition, under which the ratio of longitudinal to lateral strain is equal to Poisson's ratio.

$$\varepsilon_x = \varepsilon_y = -\nu\varepsilon_z = -\frac{\nu\sigma_y}{E} \tag{5}$$

Therefore, at the surface of the sample where the X-ray beam is incident, the following relations are valid:

$$\varepsilon_z = -\nu(\varepsilon_x + \varepsilon_y) = -\frac{\nu}{E}(\sigma_x + \sigma_y) \tag{6}$$

By combining this relation with the preceding equations, the following expression is derived:

$$\frac{d_n - d_0}{d_0} = -\frac{\nu}{E}(\sigma_x + \sigma_y) \tag{7}$$

Now, to obtain a specific stress in the Ø direction, $\sigma_\emptyset$ must be calculated. From the elastic theory for isotropic metals, it can be written as:

$$\varepsilon_{\emptyset\Psi} = \frac{1+\nu}{E}(\sigma_1 cos^2\emptyset + \sigma_2 sin^2\emptyset)sin^2\Psi - \frac{\nu}{E}(\sigma_1 + \sigma_2) \tag{8}$$

To determine the specific stress in the Ø direction, $\sigma_\emptyset$, the following expression from the theory of elasticity for isotropic materials can be used:

$$\sigma_\emptyset = \frac{E}{(1+\nu)\,sin^2\Psi}\left(\frac{d_\Psi - d_n}{d_n}\right) \tag{9}$$

Using the above relation, the residual stress on the surface at any angle can be determined by measuring the interplanar spacing in two directions—one perpendicular to the surface and the other at a specific tilt angle ψ. The most widely used method for measuring residual stress is the $sin^2\Psi$ method. In this approach, X-ray diffraction measurements are performed at various ψ angles while keeping the 2Θ angle fixed (typically greater than 100°). A graph of interplanar spacing (d) versus $sin^2\Psi$ is then plotted. Table 2 lists the specifications of the XRD device, and Fig. 3 shows the specimen prepared for the XRD test.

2.4. Simulation and optimization

The simulation in ABAQUS software was performed using the Johnson-Cook model [18], which accounts the effects of thermomechanical processes and strain rate on the distribution of residual stresses. A rectangular workpiece (3 × 8 × 12 mm) and an 8 mm four-flute end mill were modeled. The tool was designed in Catia and transferred to Abaqus for simulation. To achieve greater accuracy, a non-uniform mesh was employed, utilizing C3D8RT for the workpiece and R3D4 elements for the tool. The mechanical and thermal properties of DIN 1.2344 steel, including thermal conductivity, specific heat capacity, and the coefficient of thermal expansion, were specified.

Table 2. Specifications of the XRD device

Manufacturer	Machine model	Time step	Step length	Voltage	Current intensity	Wavelength	Anode material	Angular range	Maximum size (mm)
ASENWARE	AW-XDM300	1	0.05	40 kV	30 mAp	1.54184	Copper	160	18 × 18 × 3

The contact between the tool and the workpiece was modeled using a surface-to-surface contact approach, incorporating a temperature-dependent Coulomb friction model, as summarized in Table 3 [19-21]. Boundary conditions were applied by constraining the workpiece at its bottom face, while the tool was given a specified speed. During the simulation, the tool initially entered the workpiece slowly to stabilize the frictional conditions. Subsequently, material removal occurred at defined speeds, and variations in stress, strain, and temperature were extracted throughout the process. After the simulation, the distribution of residual stresses within the workpiece was evaluated. A comparison between the simulated and experimental XRD data showed that the residual stress variations obtained from Abaqus closely matched the experimental values, validating the numerical model. Fig. 5 illustrates the meshing method for both the tool and the workpiece.

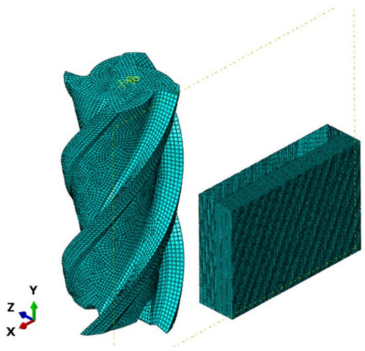

Fig. 5. The meshing method of the tool and workpiece.

Table 3. Values of Coulomb friction, Young's modulus and Poisson's ratio as a function of temperature

Temperature (˚C)	Modulus of elasticity (GPa)	Poisson's ratio	Coulomb friction
25	215	0.285	0.22
100	208	0.29	0.25
200	201	0.31	0.30
300	192	0.318	0.35
400	184	0.32	0.32
500	173	0.33	0.28

Table 4 presents the coefficients related to the Johnson-Cook equation and the damage equation, in sequence.

The simulation process in this study is carried out into two stages. In the first stage, machining is performed by rotating the tool and advancing the workpiece. The second stage involves cooling the machined surface to account for the effects of temperature changes on residual stresses. Each stage incorporates a specific loading phase or condition within the analysis, and these stages are executed sequentially to simulate the model's behavior under different conditions. In this simulation, all degrees of freedom for the tool are constrained, allowing only rotation around the tool axis. The rotational speed for the tool is assigned based on the data obtained from the design of experiments. For the workpiece, all degrees of freedom, except for the forward motion towards the tool, are constrained. The corresponding feed rate is applied according to the experimental design data. To analyze the effect of input parameters on a specified output parameter, necessary calculations must be performed using the design of experiments and the corresponding statistical relationships. In this study, the experimental design follows the Taguchi method, with Minitab software used to determine the impact of three parameters—cutting speed, feed rate, and cutting depth—on the residual stress resulting from milling. Initially, five values listed in Table 5 for each parameter are considered based on actual industrial applications in die-casting mold milling. Following the principles of the Taguchi method, this experiment includes three factors and five levels corresponding to the L25 array. Therefore, 25 experiments need to be conducted, with various combinations of cutting speeds, feed rates, and cutting depths.

Table 4. Coefficients for the Johnson-Cook equation and damage parameters [18]

Johnson-Cook equation coefficients							
A (MPa)	B (MPa)	C (MPa)	ε	n	m	T_{melt} (˚C)	T_0 (˚C)
908.54	321.39	0.028	1	0.278	1.18	1427	25
Damage equation coefficients							
D_1	D_2	D_3	D_4	D_5			
- 0.8	2.1	- 0.5	0.002	0.61			

Minitab software determines which parameter values should be combined for each experiment. The design of experiments using the Taguchi method systematically selects the number and type of factors, as well as their levels, to evaluate their effects on the process. By analyzing the data from these experiments, the optimal combination of factor levels can be identified, which helps reduce variance and improve the process performance. Optimizing experiments through the Taguchi method allows for a precise and systematic determination of the impact of each factor and control condition on the output parameter, enabling necessary adjustments in the milling process to enhance quality and performance. In this stage, the corresponding experiments are defined by the software, and the values for cutting speed, feed rate, and cutting depth to be simulated are specified

3. Results and Discussion

Fig. 6 shows the chip removal process in the simulation. One of the key criteria for ensuring the accuracy of the performed simulation and its alignment with real-world conditions is the examination of the chip formation and its geometric shape. The significance of chip formation in the simulation arises from the fact that the shape of the chip is a function of both the mechanical and thermal properties of the material, as well as the machining conditions, it can be inferred that the simulation is accurate.

From the comparisons made, a strong correlation between the chip shape obtained in the simulation and the real test conditions was observed, supporting the validity of the simulation model. As previously described, the simulation is carried out in two stages: the first stage involves the machining process, and the second stage involves cooling and heat transfer within the workpiece. After completing both stages, the residual stresses induced by the machining process are extracted and calculated as outputs in the software. Fig. 6 shows the residual stresses generated by milling on the surface of the workpiece, providing a visual representation of the stress distribution resulting from the milling operation.

According to predictions, the residual stresses induced by milling show a strong dependence on the three main machining parameters: cutting speed, feed rate, and cutting depth.

After running simulations in Abaqus under various machining conditions, the resulting residual stress values were imported into Minitab software to analyze their relationship with these parameters. The results were presented in the form of charts, organized by residual stress levels. Fig. 7 shows the effects of cutting speed, feed rate, and cutting depth on the residual stresses generated during the milling process. In this study, the experimental conditions involved measuring the temperature and pressure during the milling process, which were then compared with the simulation results. Temperature was recorded in real-time using a handheld infrared thermometer. The comparison shows minimal differences between the measured and simulated temperature values, with an average deviation of approximately 2 °C, indicating high simulation accuracy. Similarly, pressure data exhibited close agreement, with only minor discrepancies observed. These small differences may be attributed to experimental uncertainties such as slight tool geometry variations, ambient environmental factors, or limitations in measurement accuracy.

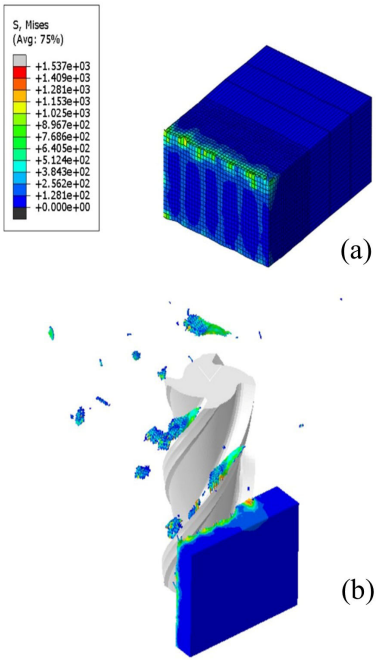

Fig. 6. (a) The residual stress caused by milling and (b) the method of chip removal in the simulation.

Overall, the strong correlation between experimental and simulated results confirms the reliability of the simulation model in predicting both temperature and pressure during the milling process Therefore, the model can be confidently employed for process optimization and further analysis, particularly in machining materials like titanium or steel. Fig. 8 presents the comparison of experimental and simulated pressure and temperature across various milling parameters. As shown in the graph trend, residual stress initially increases with rising cutting speed. However, this rate of increase slows down, and a cutting speed of 112.5 mm/min, the trend reverses residual stress begins to decrease and continues to do so across the remainder of the experimental range. This shift can be attributed to competing effects between strain rate and thermomechanical phenomena.

At lower cutting speeds, increasing the speed raises the strain rate, which in turn generates higher residual stresses in the workpiece. However, as cutting speed continues to rise, the influence of thermomechanical effects—such as heat generation and thermal expansion becomes dominant, eventually outweighing the strain rate effects and leading to a reduction in residual stress. The relationship between cutting speed and residual stress is inherently complex, influenced by various factors including material properties, machining conditions, tool geometry, and cutting parameters. Nonetheless, strain rate and thermomechanical effects are the primary contributors. With bigger cutting speed, increased friction at the tool–chip interface generates more heat, causing localized thermal expansion in the workpiece.

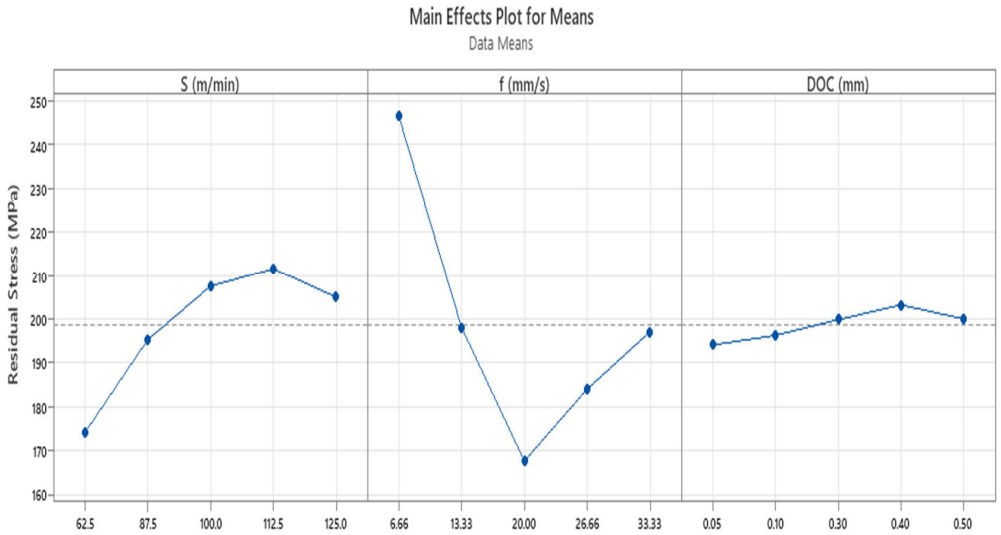

Fig. 7. The effect of milling parameters on residual stress.

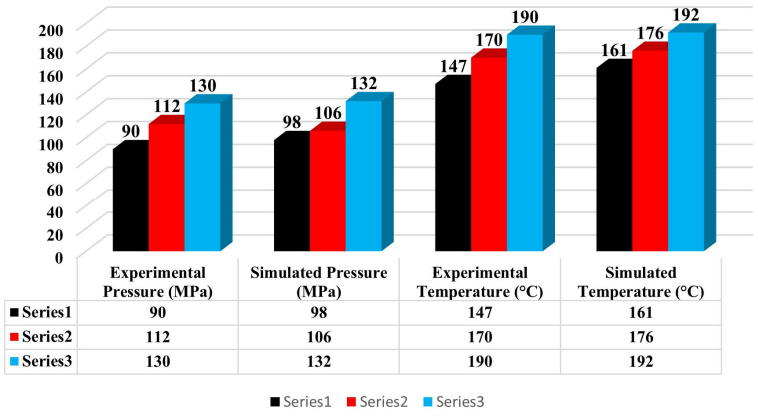

Fig. 8. Comparison between experimental and simulated temperature and pressure under various milling parameters.

Subsequent rapid cooling results in contraction, introducing thermal stresses that can alter the microstructure and contribute to residual stress formation. Simultaneously, the elevated strain rates at higher speeds further affect the material's crystalline structure. The material's sensitivity to strain rate thus plays a crucial role in determining the resulting residual stress levels. Rapid deformation and strain can alter the material's crystalline structure, resulting in the generation of residual stresses. The sensitivity of the material's strain rate plays a key role in determining the level of residual stress generated. As observed in the trend of the graph, with an increase in feed rate, the resulting residual stress values decrease. However, the rate of change slows down with increasing feed rate, until at a feed rate of 20 mm/s, the residual stress trend with respect to feed rate becomes increasing, and this increasing trend persists throughout the experimental range. The cause of this change, similar to the trend observed for cutting speed, can be related to variations in strain rate and the thermomechanical phenomenon, with the difference being that the effect of feed rate on changes in strain rate and thermomechanical effects differs across various ranges. The reverse trend of residual stress changes with respect to feed rate, as compared to cutting speed, is due to the differing influence of these two parameters on the changes in strain rate and thermomechanical effects.

At low feed rates, the thermomechanical effect dominates, and with the gradual increase in feed rate, the effect of increasing strain rate on thermomechanics becomes more significant, leading to an increase in residual stresses. Similar to cutting speed, the relationship between feed rate and residual stresses is complex and depends on various factors. The feed rates can reduce the time during which the material is exposed to the heat generated during cutting, potentially minimizing residual stresses associated with thermal effects. Higher feed rates can reduce the time during which the material is exposed to the heat generated during cutting, potentially minimizing residual stresses associated with thermal effects. On the other hand, a lower feed rate may result in a longer contact time, potentially allowing more heat to accumulate and increasing the likelihood of thermal stress formation. Additionally, the feed rate directly impacts the material removal rate. A higher feed rate leads to faster material removal, which can help minimize the area affected by heat—an area most likely to experience thermal stresses. The feed rate also affects chip formation. Higher feed rates generally result in thinner and more continuous chips. The way chips are separated can increase cutting forces and heat generation. Poor chip control can contribute to higher residual stresses.

It is important to note that different materials respond differently to changes in feed rate. Some materials may be more sensitive to the formation of residual stresses due to variations in cutting speed, while others may exhibit less sensitivity. These tendencies can also be predicted using the material-specific coefficients in the Johnson-Cook equation.

As observed in the graph trend, with an increase in cutting depth, the resulting residual stress values also increase. However, the rate of increase becomes more gradual as the cutting depth continues to rise, until at approximately 0.4 mm, the trend reverses and residual stresses begin to decrease. This decreasing trend continues throughout the remainder of the experimental range. Compared to cutting speed and feed rate, cutting depth has a less significant influence on residual stresses formation. Cutting depth affects the amount of material exposed to heat during machining. Deeper cuts result in prolonged contact between the tool and the workpiece, leading to increased thermal input and the potential for elevated thermal stresses. While reducing the cutting depth may help mitigate thermal effects, deeper cuts enhance chip removal rates, which can increase machining efficiency but also elevate the risk of heat accumulation and associated thermal stresses.

Additionally, cutting depth impacts chip formation, particularly the thickness and type of chips produced. Deeper cuts generally generate thicker chips, and if chip control is inadequate, re-cutting of chips may occur. This can increase cutting forces and heat generation, further influencing the residual stress profile. The response of a material to changes in cutting depth also depends on its

inherent properties; some materials may be more susceptible to residual stress development under varying cutting depths, while others may be relatively insensitive [22]. In summary, cutting depth is a critical machining parameter that can significantly affect residual stress generation. While deeper cuts enhance material removal efficiency, they also raise the risk of thermal stress and tool wear. Therefore, cutting depth must be carefully optimized in conjunction with other machining parameters to achieve the desired surface integrity, dimensional accuracy, and minimized residual stress. To validate the simulation results, experimental tests were conducted using the X-ray diffraction method. A total of six tests were performed on three samples, in two orthogonal directions, to calculate the von Mises residual stresses. The experimental results were compared with those obtained from simulation, and a strong agreement was observed, confirming the accuracy of the numerical model. Table 5 presents the results from the experimental tests.

Table 5. Residual stress results from XRD tests on three samples in two directions

Sample	S (m/min)	f (mm/s)	DOC (mm)	Residual stress (MPa)
1	62.5			122.69
2	100	26.66	0.4	179.38
3	125			173.624

The trend of residual stresses obtained from both simulation and experimental testing as a function of cutting speed is consistent, confirming the reliability of the simulation model. In both datasets, with constant feed rate and cutting depth, residual stresses initially increase with cutting speed and subsequently decrease beyond a certain point. These variations have been discussed in detail in earlier sections.

Fig. 9 presents the residual stress analysis results, measurement angles, and a comparison between experimental and simulation data.

In the Taguchi analysis, the signal-to-noise (S/N) ratio summarized in Table 6, is used to evaluate the robustness of the machining process. Taguchi's method aims to identify parameter settings that minimize the impact of variability and external disturbances, thereby enhancing process stability and quality. In this study, the optimal combination of machining parameters for minimizing residual stress was determined. The results show that a high cutting speed (125 m/min) combined with a moderate feed rate (20 mm/s) effectively reduces residual stress. The signal-to-noise (S/N) ratio further confirms the influence and sensitivity of each parameter [23]. Overall, the analysis indicates that increasing cutting speed while reducing cutting depth contributes significantly to residual stress reduction and process optimization. To assess the statistical significance of each parameters' effect on residual stress, an analysis of variance (ANOVA) was conducted. The results are summarized in Table 7.

Cutting speed: The F-value for cutting speed is very high (15.5) and the p-value is very small (0.0005), indicating that this parameter has a statistically significant effect on the results. This suggests that cutting speed has a substantial impact on the desired characteristics of the milling process.

Feed rate: The F-value for feed rate is 10.3, with a p-value of 0.002, which also confirms a statistically significant effect. Although its impact is slightly lower than that of cutting speed, feed rate still plays an important role in determining milling outcomes.

Table 6. Taguchi analysis results: signal-to-noise ratios for residual stress under different machining parameter

Experiment No.	Residual stress (MPa)	S/N ratio	Optimal parameters
1	69.122	4.0	Cutting speed: 62.5 m/min, Feed rate: 6.66 mm/s, Cut depth: 0.05 mm
2	38.179	4.5	Cutting speed: 100 m/min, Feed rate: 13.33 mm/s, Cut depth: 0.10 mm
3	624.173	5.0	Cutting speed: 125 m/min, Feed rate: 20 mm/s, Cut depth: 0.30 mm
4	345.100	5.2	Cutting speed: 112.5 m/min, Feed rate: 26.66 mm/s, Cut depth: 0.40 mm
5	543.156	4.8	Cutting speed: 87.5 m/min, Feed rate: 33.33 mm/s, Cut depth: 0.50 mm

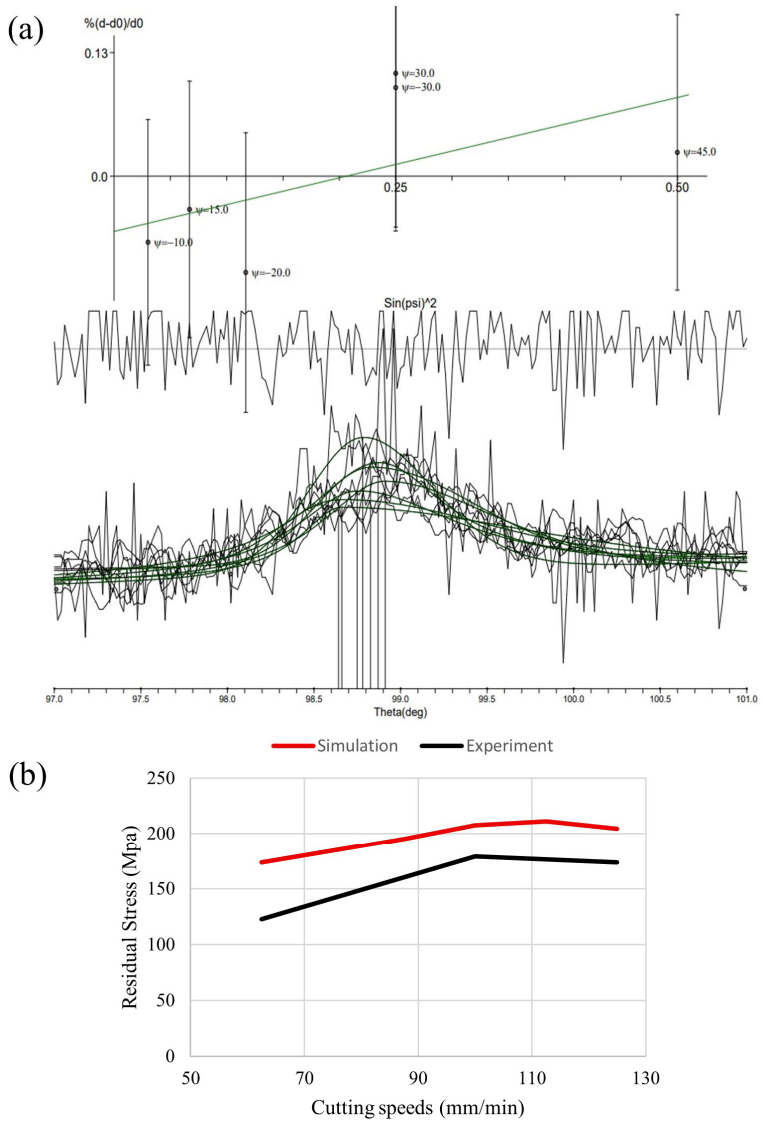

Fig. 9. (a) Measurement angles and comparison between experimental test results and simulation, (b) residual stress analysis results.

Table 7. ANOVA results: effects of milling parameters on residual stress

Factor	Sum of squares	df	Mean square	F-value	p-value
Cutting speed (m/min)	1200	2	600	15.5	0.0005
Feed rate (mm/s)	800	2	400	10.3	0.002
Depth of cut (mm)	400	2	200	5.2	0.015
Pure error	1000	8	125		
Cor total	3400	14			

Cut Depth: The F-value for cut depth is 5.2, and the p-value is 0.015, indicating a significant effect, though less pronounced than that of cutting speed and feed rate. However, cut depth remains a meaningful factor in process optimization.

Error: The error term shows a low F-value and a high p-value, indicating that the statistical error has a minimal effect on the results. This suggests that the model fits the data well, and that the observed effects are primarily attributable to the investigated parameters. Based on this analysis, it is evident that all three parameters—cutting speed, feed rate, and cut depth—significantly influence the outcomes of the milling process. Among them, cutting speed exhibits the most pronounced effect. Although feed rate and cut depth also impact the results, their effects are comparatively less substantial. These findings offer valuable insights for optimizing milling parameters and enhancing the quality

of the manufactured components.

Residual stress measurements were performed using X-ray diffraction, focusing on the peak at 98.7° within a scan range of 97° to 101°. Measurements were taken at ψ angles of -10°, -20°, -30°, 0°, 15°, 30°, and 45°, with scans starting at 68° and using a step size of 0.02°. The intensity at each peak was recorded to evaluate residual stress distribution.

$$\varepsilon_{\emptyset\Psi} = \frac{1+\nu}{E}(\sigma_1 cos^2\emptyset + \sigma_2 sin^2\emptyset)sin^2\Psi - \frac{\nu}{E}(\sigma_1 + \sigma_2) \quad (10)$$

In milling operations, the interaction between the tool and workpiece generates milling forces due to continuous material removal. These forces are strongly influenced by machining parameters, including cutting speed, feed rate, and cutting depth as well as the material properties of the workpiece, all of which are interrelated with the development of residual stresses. Assuming a coordinate system as illustrated in Fig. 10(a), the variations of milling forces F_x, F_y, and F_z with respect to cutting speed and feed rate are presented in Figs. 10(b) and 10(c). However, as the cutting speed exceeds approximately 0.5 mm/min, the forces begin to decrease a behavior primarily attributed to thermal softening, which reduces material strength at elevated temperatures. While F_y exhibits a similar general trend, its magnitude and variation are significantly smaller compared to F_x and F_z, suggesting a lesser role in the primary cutting direction. Additionally, milling forces also vary with feed rate in a manner consistent with cutting speed, showing that both parameters critically influence cutting stability and surface quality (Fig. 10).

As observed in the graph, all three force components F_x, F_y, and F_z increase with the rise in feed rate, although they exhibit varying rates of change. Among them, the F_x component shows the most significant fluctuations due to its directional orientation relative to the cutting motion. Compared to cutting speed, feed rate has a more pronounced impact on milling forces. Similar to the trend observed for cutting speed, the force variation with respect to feed rate initially progresses gradually; however, as the feed rate increases further, the rate of change in forces becomes more substantial.

As shown in the graph, all three forces F_x, F_y, and F_z increase with the rise in feed rate, though their rates of change differ.

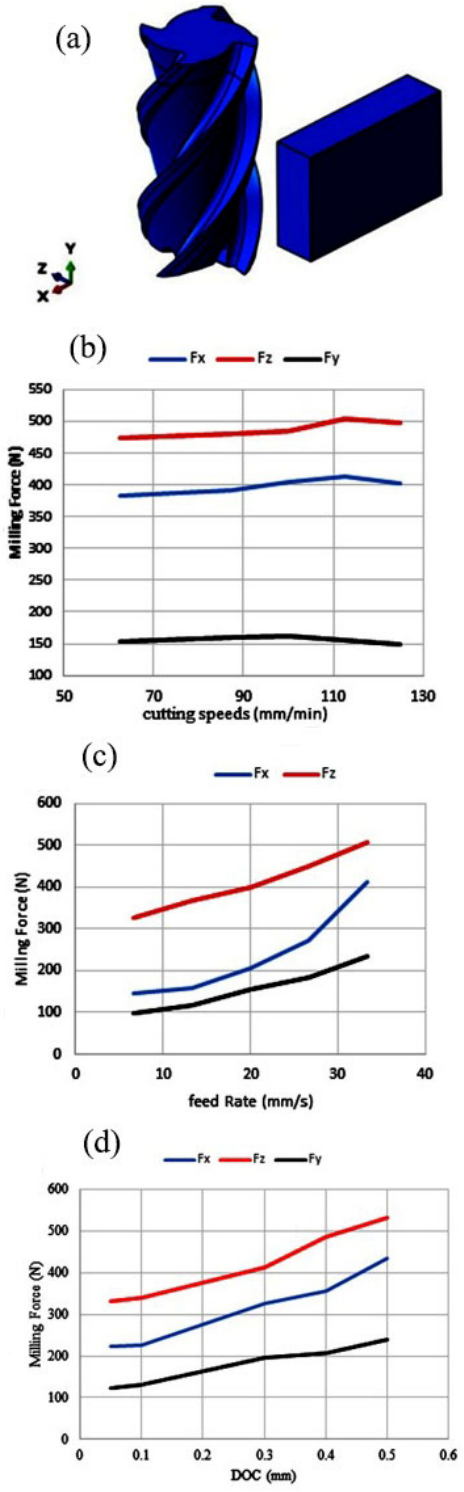

Fig. 10. (a) Coordinate directions used in the simulation, (b, c) variations of milling forces with different cutting speeds and feed rates, and (d) variations of milling forces at different cutting depths.

The increase in milling forces with increasing cutting depth is consistent across the entire simulation range. The variations are especially pronounced, indicating that cutting depth has a more significant impact on milling forces than cutting speed and feed rate. As the cutting depth increases, the cutting force required to remove material also rises. This is due to the fact that a deeper cut requires the tool to engage a larger volume of material in each pass, thereby increasing the mechanical load and resulting forces [24].

4. Conclusions

1. With an increase in cutting speed, the residual stresses initially increase, but at a cutting speed of 112.5 m/min, this trend reverses and starts to decrease.
2. An increase in feed rate initially causes a reduction in residual stresses, but at a feed rate of 20 mm/s, this trend reverses and begins to increase.
3. An increase in cutting depth initially leads to an increase in residual stresses, but at a cutting depth of 0.4 mm, this trend changes and starts to decrease.
4. Feed rate, cutting speed, and cutting depth, in that order, have the most significant impact on the residual stresses caused by milling in the DIN 1.2344 alloy.
5. The residual stresses resulting from milling are dependent on the material properties and milling parameters such as cutting speed, feed rate, and cutting depth.
6. At low cutting speeds, the sensitivity to strain rate is higher, while at high cutting speeds, the effects of thermal softening become more pronounced.
7. The reversal of residual stress trends with changes in cutting speed and feed rate is due to the different effects of these two parameters on strain rate and the thermal softening phenomenon.
8. The minimum residual stresses in the DIN 1.2344 alloy are achieved with cutting speeds of 62.5 m/min, feed rates of 20 mm/s, and cutting depths of 0.05 mm.

Acknowledgements

The authors are deeply grateful to all those who played a role in the success of this research.

Conflict of interest

The authors declare no financial interests or personal relationships that could have influenced the findings presented in this study.

Funding

This research was conducted without any financial support.

5. References

[1] Yang, J., Liu, B., Zeng, Y., Zhang, Y., Huang, H., & Hong, J. (2024). Data extension-based analysis and application selection of process-composition-properties of die casting aluminum alloy. *Engineering Applications of Artificial Intelligence*, *133*, 108514. https://doi.org/10.1016/j.engappai.2024.108514

[2] Peti, F., & Grama, L. (2011). Analyze of the possible causes of porosity type deffects in aluminium high pressure diecast parts. *Acta Marisiensis. Seria Technologica*, *8*(1), 41.

[3] Klobčar, D., Tušek, J., & Taljat, B. (2007). Thermal fatigue of materials for die-casting tooling. *Materials Science and Engineering: A*, *472*(1–2), 198–207. https://doi.org/10.1016/j.msea.2007.03.025

[4] Dawim, J. P. (2010). *Metal cutting: Research advances*. Nova Science Publishers.

[5] Fuh, K. H., & Wu, C. (1995). A residual-stress model for the milling of aluminum alloy (2014-T6). *Journal of Materials Processing Technology*, *51*(1–4), 87–105. https://doi.org/10.1016/0924-0136(94)01355-5

[6] Demirpolat, H., Binali, R., Kuntoğlu, M., Salur, E., Makhesana, M. A., Yaghoubi, S., & Usca, Ü. A. (2024). The influences of alloying elements and processing conditions on the machinability of wrought aluminium alloys: A literature review. *Proceedings of the Institution of Mechanical Engineers, Part E: Journal of Process Mechanical Engineering*. https://doi.org/10.1177/09544089241290395

[7] Liang, S., & Su, J. C. (2007). Residual stress modeling in orthogonal machining. *CIRP Annals*, *56*(1), 65–68. https://doi.org/10.1016/j.cirp.2007.05.018

[8] Honarpisheh, M., & Mansouri, H. (2018). Experimental study of residual stress on TIG welding of CK45 sheet by contour method. *International Conference on Manufacturing Engineering,* Tehran, Iran. https://civilica.com/doc/837818

[9] Mohammadpour, M., Razfar, M. R., & Saffar, R. J. (2010). Numerical investigating the effect of machining parameters on residual stresses in orthogonal cutting.

Simulation Modelling Practice and Theory, *18*(3), 378–389. https://doi.org/10.1016/j.simpat.2009.12.004

[10] Stenberg, N., & Proudian, J. (2013). Numerical modelling of turning to find residual stresses. *Procedia CIRP*, *8*, 258–264. https://doi.org/10.1016/j.procir.2013.06.099

[11] Kara, M. E., Kuzu, A. T., & Bakkal, M. (2024). Investigation of residual stresses induced by milling of compacted graphite iron by x-ray diffraction technique. *Journal of Materials Engineering and Performance*, *33*(8), 3801–3810. https://doi.org/10.1007/s11665-023-08904-3

[12] Zhou, J., Qi, Q., Liu, Q., Wang, Z., & Ren, J. (2024). Determining residual stress profile induced by end milling from measured thin plate deformation. *Thin-Walled Structures*, *200*, 111862. https://doi.org/10.1016/j.tws.2024.111862

[13] Fergani, O., Barka, N., Chatti, S., & Dogui, A. (2014). Analytical modeling of residual stress and the induced deflection of a milled thin plate. *The International Journal of Advanced Manufacturing Technology*, *75*, 455–463. https://doi.org/10.1007/s00170-014-6146-3

[14] Abidi, Y., Mokas, N., & Kerdoun, D. (2024). Contribution to practical analysis of surface roughness modeling during dry hard turning of cold work tool steel AISI D2. *Surface Review and Letters*, *31*(09), 2450071. https://doi.org/10.1142/s0218625x24500719

[15] Nalbant, M., Gökkaya, H., & Sur, G. (2007). Application of Taguchi method in the optimization of cutting parameters for surface roughness in turning. *Materials & Design*, *28*(4), 1379-1385. https://doi.org/10.1016/j.matdes.2006.01.008

[16] Pınar, A. M., Filiz, S., & Ünlü, B. S. (2016). A comparison of cooling methods in the pocket milling of AA5083-H36 alloy via Taguchi method. *The International Journal of Advanced Manufacturing Technology*, *83*, 1431–1440. https://doi.org/10.1007/s00170-015-7666-1

[17] Zahoor, S., Mufti, N. A., Qureshi, M. Q., Saleem, M. P., & Mughal, M. A. M. (2017). Effect of machine tool's spindle forced vibrations on surface roughness, dimensional accuracy, and tool wear in vertical milling of AISI P20. *The International Journal of Advanced Manufacturing Technology*, *89*, 3671–3679. https://doi.org/10.1007/s00170-016-9346-1

[18] Timothy, N., Gomez, M., Karandikar, J., Heigel, J., Copenhaver, R., & Schmitz, T. (2021). Propagation of Johnson–Cook flow stress model uncertainty to milling force uncertainty using finite element analysis and time domain simulation. *Procedia Manufacturing*, *53*, 223–235. https://doi.org/10.1016/j.promfg.2021.06.025

[19] Debnath, S., Reddy, M. M., & Yi, Q. S. (2016). Influence of cutting fluid conditions and cutting parameters on surface roughness and tool wear in turning process using Taguchi method. *Measurement*, *78*, 111–119. https://doi.org/10.1016/j.measurement.2015.09.011

[20] Wang, C., Ma, R., Zhao, J., & Zhao, J. (2017). Calculation method and experimental study of Coulomb friction coefficient in sheet metal forming. *Journal of Manufacturing Processes*, *27*, 126–137. https://doi.org/10.1016/j.jmapro.2017.02.016

[21] Nine, H. D. (1982). The applicability of Coulomb's friction law to drawbeads in sheet metal forming. *Journal of Applied Metalworking*, *2*, 200–210. https://doi.org/10.1007/BF02834038

[22] Masoudi, S., Amini, S., Saeidi, E., & Eslami, H. (2015). Effect of machining-induced residual stress on the distortion of thin-walled parts. *The International Journal of Advanced Manufacturing Technology, 76*, 597–608. https://doi.org/10.1007/s00170-014-6281-x

[23] Chen, D. C., Jhang, J. J., & Guo, M. W. (2013). Application of Taguchi design method to optimize the electrical discharge machining. *Journal of Achievements in Materials and Manufacturing Engineering*, *57*(2), 76–82.

[24] Juneja, B. L. (2003). *Fundamentals of metal cutting and machine tools*. New Age International.